Thermal Reduction of Cu^{2+}−Mordenite and Re-oxidation upon Interaction with H_2O, O_2, and NO

F. X. Llabrés i Xamena, P. Fisicaro, G. Berlier, and A. Zecchina

Department of Inorganic, Physical and Materials Chemistry, University of Turin, Via Giuria 7, 10125 Torino, Italy, and INSTM UdR Torino Università

G. Turnes Palomino

Departamento de Química, Universidad de las Islas Baleares, 07071 Palma de Mallorca, Spain

C. Prestipino, S. Bordiga, E. Giamello, and C. Lamberti*

Department of Inorganic, Physical and Materials Chemistry, University of Turin, Via Giuria 7, 10125 Torino, Italy, INSTM UdR Torino Università, and INFM UdR Torino Università

Received: November 29, 2002

We present a multitechnique (EPR, XANES, EXAFS, and IR of adsorbed NO) study of the coordination and oxidation chemistry of copper species hosted in mordenite (MOR) zeolite under different conditions. Starting from a 100% Cu^{2+}−MOR, the progressive thermal activation causes first the loss of water molecules from the Cu^{2+} coordination sphere, accompanied by a partial aggregation in Cu^{2+}−O−Cu^{2+} complexes, and then the $Cu^{2+} \rightarrow Cu^{+}$ reduction with oxygen elimination. The presence of EPR inactive cupric pairs, witnessed by EXAFS, explains the systematic underestimation of the fraction of Cu^{2+} species evaluated by EPR, with respect to that obtained from XANES. The data discussed here confirm the interpretation of the so-called "self-reduction" phenomenon of cupric ions emerging in a previous study performed on Cu−ZSM-5 [*J. Phys. Chem. B* **2000**, *104*, 4064]. The reoxidation of the so obtained Cu^{+}−MOR by O_2 is dramatically favored by the presence of water. This fact explains the poisoning effect of water in the deNO_x activity of Cu-exchanged zeolites. The coordination of NO molecules on the Cu^{+}−MOR system was studied in situ at liquid nitrogen temperature. The deNO_x chemistry was then switched on by allowing the system to reach room temperature in the NO atmosphere. In all stages of this study, comparison is made with a Cu^{+}−ZSM-5 model system. The differences observed between these two systems are explained in terms of the different structural (cation concentration and environment) characteristics.

1. Introduction

In recent years, copper-exchanged zeolites have attracted much attention owing to their high catalytic performance in the direct decomposition of nitric oxide into nitrogen and oxygen.[1−5] This process deserves a considerable practical interest, as nitrogen oxides are considered to be a major cause of air pollution. Knowledge on the oxidation and coordination state of copper ions in zeolites, under various experimental conditions, is essential to understand the nature of the active centers in the working catalyst. Several papers devoted to this aim have appeared recently on both experimental[6−22] and computational[23−25] grounds. In particular, much attention was focused on the study of the redox chemistry of copper ions inside the zeolite framework. For instance, it is well-known that hydrated Cu^{2+} species in copper-exchanged zeolites undergo a progressive reduction upon thermal treatment under *vacuum* at increasing temperatures[26−36] However, some discrepancies exist in the interpretation of the experimental results. Indeed, two main mechanisms were proposed to explain this behavior of copper ions, the often called "self-reduction" process.

The first mechanism consists of the condensation of two $Cu(OH)^{+}$ neighboring species with elimination of a water molecule, and with attendant formation of $Cu^{2+}O^{2-}Cu^{2+}$ moieties. In a consecutive step, reduction of both Cu^{2+} ions is achieved, giving rise to $Cu^{+}\square Cu^{+}$ centers, where the symbol $\square$ stands for a vacancy of an extralattice oxygen; see eq 1.

$$2[CuOH]^{+} \rightarrow Cu^{2+}O^{2-}Cu^{2+} + H_2O \rightarrow Cu^{+}\square Cu^{+} + {}^{1}/_{2}O_2 \quad (1)$$

As pointed out by Iwamoto et al.,[1−5] such extralattice oxygen species can be introduced into the zeolite framework during the ion exchange process. The extralattice oxygen is eliminated by desorption of O_2. Jong et al.[32] discussed this phenomenon in terms of the sublimation pressure of O_2 with consequent formation of Cu^{+} ions, and assigned a low-frequency IR band (at 910 cm^{-1}) to oxygen extralattice species.

The second mechanism, proposed by Larsen et al.,[34] is based on water elimination and formation of hydroxyl radicals ($^{\bullet}OH$) and O^{-} ions. According to this mechanism, a fraction of copper is reduced, but a second fraction still remains as Cu^{2+} ions, in the form of $Cu^{2+}O^{-}$ pairs.

* To whom correspondence should be addressed. Fax: +39011-670-7855. E-mail: carlo.lamberti@unito.it.

10.1021/jp0275847 CCC: $25.00
Published on Web 06/25/2003

$$Cu^{2+}OH^- \rightarrow Cu^+ + {}^{\bullet}OH \quad (2)$$

$$Cu^{2+}OH^- + {}^{\bullet}OH \rightarrow Cu^{2+}O^- + H_2O \quad (3)$$

$$2[Cu^{2+}OH^-] \rightarrow Cu^+ + Cu^{2+}O^- + H_2O \quad (4)$$

This mechanism was proposed on the basis of electron paramagnetic resonance (EPR) data, which showed that the intensity of the Cu^{2+} EPR signal diminished upon thermal treatment under a vacuum and was restored by simple addition of water even at room temperature. However, this hypothesis was confuted by Lo Jacono et al.,[35] who suggested that the loss of the EPR signal was not actually due to the diminution of the amount of Cu^{2+} ions, but to changes in the coordination of Cu^{2+} ions upon thermal treatment, giving rise to EPR-silent species (such as dimeric Cu^{2+} moieties), without formation of cuprous ions.

In a recent work, we used FTIR, UV−vis, EPR, XANES, and EXAFS spectroscopies to study the thermal reduction and reoxidation by water and oxygen of copper ions in Cu-exchanged ZSM-5 zeolites.[36] Our results were in agreement with a two-step reduction process: the first part of the thermal treatment (between room temperature and 473 K) produces (mainly) the loss of water, without appreciable reduction of Cu^{2+} ions, as testified by XANES. The dehydration is accompanied by a rearrangement of the cupric species inside the zeolitic channels, a fraction of which becomes EPR silent, as suggested by the presence of a Cu−Cu component in the Fourier transform of EXAFS data typical of Cu^{2+} dimmers. Further increasing the temperature (from 473 up to 673 K) causes oxygen elimination and reduction of cupric ions to Cu^+, as stated by the combined XANES/EPR study. XANES and EXAFS of the reduced sample showed that at room-temperature water molecules coordinate to Cu^+ ions but, despite an observed increase of the EPR signal, they are not able to reoxidize Cu^+ ions to Cu^{2+}. The observed increment of the EPR signal is most probably due to the rearrangement of previously silent Cu^{2+} species already present in the partially reduced sample, and not to a reoxidation of cuprous ions by water. However, water facilitates reoxidation by molecular oxygen at room temperature. Indeed, oxidation by oxygen in a dehydrated environment is an activated process and does not take place at room temperature. In conclusion, our previous results[36] gave strong evidence in favor of the first proposed mechanism of thermal reduction, eq 1.

An other important aspect of the redox chemistry of copper in zeolites is related to the oxidative interaction of NO molecules with Cu^+ ions, being strictly related to the abatement of NO_x pollutants.[8,13−16,18,22,37,38]

In the present work, we extended our studies to another zeolitic system; i.e., copper-exchanged mordenite,[30,39] so as to verify if the results obtained with ZSM-5 zeolites are of general application. Results will thus be compared with those previously obtained with ZSM-5, taking into account that some structural differences exist between these two systems. On one hand, a smaller Si/Al ratio is present in mordenite (and thus, its copper content is higher) as compared to ZSM-5. On the other hand, mordenite contains cation sites having different chemical environments and accessibility (i.e., in the main channels and in the side-pockets), which is in contrast with ZSM-5 where all cations are equally accessible and are more alike (vide infra section 3.3.1 for a more detailed description).

2. Experimental Section

The starting H-mordenite sample used (Si/Al = 5) was kindly supplied by *Polimeri Europa S.p.A., Istituto G. Donegani.* X-ray powder diffraction showed good crystallinity and confirmed the MOR structure type.[40] No additional diffraction lines belonging to other phases were detected. This material was ion-exchanged two times with a 0.4 M $Cu(NO_3)_2$ aqueous solution at room temperature for 3 days. The resulting copper-exchanged mordenite will be hereafter termed Cu−MOR. By comparing the intensity of the IR band at 3610 cm^{-1} (characteristic of the O−H stretching mode of framework Si−OH−Al groups[41]) prior to and after the exchange, the extend of ion-exchange for this sample was evaluated to be almost complete.

X-band EPR spectra were recorded at 77 K on a Brucker EMX spectrometer equipped with a dual cavity always employing the same set of instrumental parameters. The quartz cell used was designed to allow in situ thermal treatment of the sample, gas dosage, and spectra recording at low temperature to be carried out.

For FTIR studies, a portion of the sample Cu−MOR was pressed into a thin self-supported wafer and activated under a vacuum at 673 K for 2 h inside an IR cell, which allows in situ thermal treatments, gas dosage, and low-temperature measurements to be carried out.

X-ray absorption measurements (experiment CH-1015[42]) were performed at the GILDA BM8 beamline[43] at the European Synchrotron Radiation Facility (ESRF). The monochromator used was equipped with two Si(311). Harmonic rejection was achieved using mirrors. The geometry of the beamline was optimized to improve the energy resolution and to obtain very high quality XANES spectra: vertical slits, located at 23 m from the source, were set to 0.5 mm to ensure an energy resolution better than 0.4 eV at 9 keV. The experimental geometry adopted was as follows: 1) I_0 (1 bar N_2 filled ionization detector having efficiency of 10%); 2) zeolite sample; 3) I_1 (100 mbar Ar filled ionization detector having efficiency of 50%); 4) 7 μm thick copper metal foil; 5) I_2 (photodetector). The first maximum of the XANES derivative spectrum of the Cu metal foil (the 1s → 4p electronic transition of Cu^0) was defined as 9879.0 eV. A sampling step of 0.2 eV for the XANES part of the spectra and a variable sampling step, giving $\Delta k_{max} = 0.05$ Å^{-1} for the EXAFS part and an integration time of 3 s/point were adopted. Spectra were collected at room temperature (except for the case of NO, vide infra), using a metallic cell allowing in situ treatments up to 800 K and gas dosage to be carried out. For each sample three equivalent spectra were collected, and extracted $\chi(k)$ were averaged before the EXAFS data analysis.[44] The EXAFS data analysis was performed following standard procedures.[45]

The following experimental procedure was adopted: Cu^{2+}-exchanged mordenite was activated under dynamic vacuum at increasing temperature: 300, 373, 473, 573, and 673 K for 1 h. XANES and EXAFS spectra were collected after each activation step. The sample activated at 673 K was exposed to the vapor pressure of H_2O at room temperature (equilibrium pressure of ca. 12 Torr) for 2 h. After the corresponding spectra were collected, O_2 was admitted (equilibrium pressure of ca. 100 Torr) on the hydrated sample and a second series of XANES and EXAFS was recorded. In a separate experiment, NO was dosed onto a freshly prepared wafer of Cu−MOR activated at 673 K as before ($P_{NO} = 8$ Torr). NO dosage was carried out at the liquid nitrogen temperature to avoid the oxidation of Cu^+ cations. The temperature of the sample was then allowed to increase up to 300 K in NO atmosphere, and finally, the system was outgassed at room temperature. After each step, a series of EXAFS and XANES was collected. The same procedure was followed in our laboratories for the EPR and FTIR experiments.

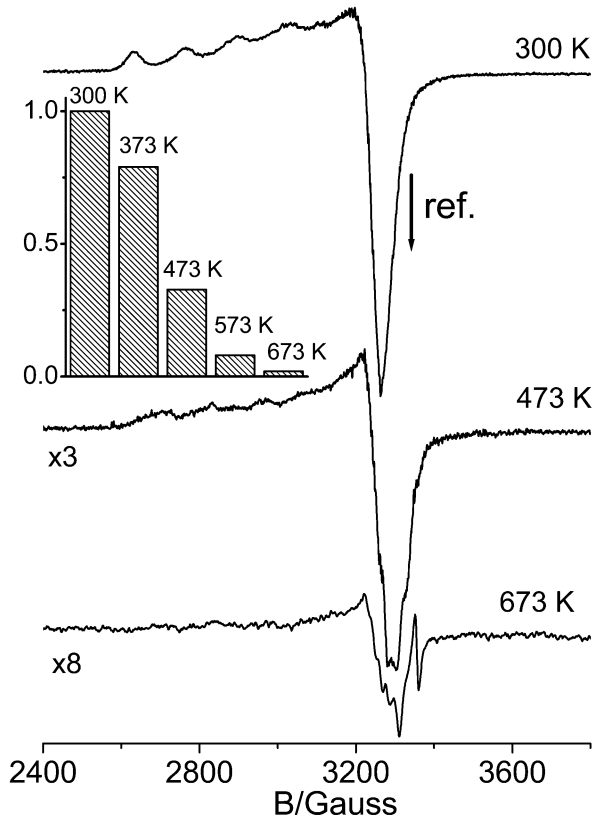

Figure 1. EPR spectra, recorded at 77 K, of Cu−MOR activated at increasing temperatures from 300 to 673 K. Only three spectra are shown for clarity. The inset reports the relative integrated intensities of the EPR signal of all the spectra, referred to that of the sample activated at 300 K. The vertical arrow refers to the free spin value ($g_e = 2.0023$).

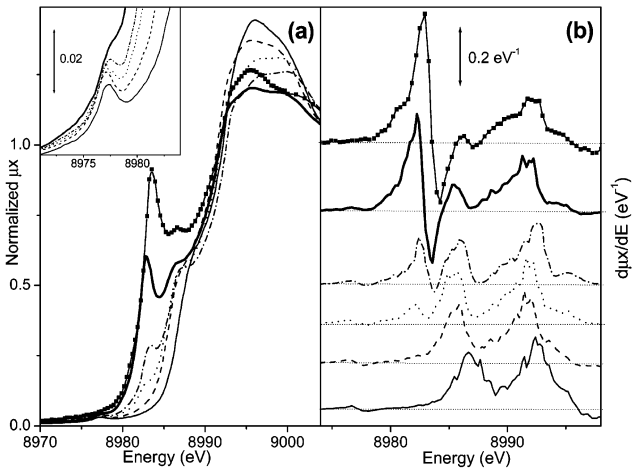

Figure 2. (a) XANES spectra of Cu−MOR thermally treated at increasing temperatures: 300 K (full line), 373 K (dashed line), 473 K (dotted line), 573 K (dotted-dashed line), and 673 K (bold full line). For comparison the spectrum of a Cu^+−ZSM-5 model compound (line-square curve) is also included (from ref 22). The inset reports the magnification of the 1s → 3d electronic transition of Cu^{2+} species. (b) Corresponding derivative spectra (same drawing as in part a). For the sake of clarity spectra were vertically shifted. For every curve a horizontal dotted line represents the corresponding zero level.

3. Results and Discussion

3.1. Thermal "Self-Reduction" of Cu^{2+} in Cu−MOR under a Vacuum. *3.1.1. EPR Spectroscopy.* The EPR spectrum of the as-prepared Cu−MOR sample (not shown for brevity) is typical of hydrated Cu^{2+} ions. When recorded at 77 K, a broad axial signal with scarcely resolved parallel hyperfine structure is observed. The spectrum recorded at room temperature tends to be isotropic and still less resolved than the 77 K spectrum, which suggests a partial mobility of the hydrated cupric species.

The effect of the thermal treatments under vacuum at increasing temperature (from 300 to 673 K) is shown in Figure 1, where only three spectra out of five are presented for clarity. Upon an increase in temperature, a diminution of the intensity of the EPR signal and a partial increase of the resolution of the components is observed. In the inset, the relative integrated intensities of all the EPR spectra are presented. For the calculation of these values, the intensity of the starting sample was assumed to be 1, and all the other intensities are referred to this value. As observed in the figure, the intensity of the EPR signal is reduced down to ca. 2% of the initial value after the sample is evacuated at 673 K.

From the above observed intensity diminution, it could be inferred that an almost complete reduction of Cu^{2+} to Cu^+ ions is taking place upon outgassing the Cu−MOR sample at increasing temperature, as was the case of Cu−ZSM-5 zeolite activated in the same way.[36] Note, however, that this conclusion is not straightforward, on account of the fact that Cu^{2+} EPR-silent species can also be present (e.g., $Cu^{2+}O^{2-}Cu^{2+}$ diamagnetic pairs[14,27,35,36]), which can be formed by a rearrangement of cupric ions upon water loss. We will come again to this point in the following.

3.1.2. High-Resolution XANES. Owing to the atomic selectivity and sensitivity to both local environment and oxidation state of Cu species, several groups used XANES to characterize the oxidation and aggregation states of copper species in zeolites in various conditions and after interaction with adsorbates.[8,18−22,30,36,46−49] The assignment of the main XANES features of Cu^+ and Cu^{2+} species in zeolites was recently summarized in ref 22. Without entering in the detail, we shall recall here only that a single well-defined peak at 8983−8984 eV is the fingerprint of Cu^+ species due to the dipole-allowed 1s → 4p electronic transition. On the contrary, Cu^{2+} species exhibit a weak absorption at about 8976−8979 eV, attributed to the dipole-forbidden 1s → 3d electronic transition and a shoulder at about 8986−8989 eV due to 1s → 4p transitions.[8,19,22,30,31,50]

Figure 2a reports the XANES spectra of the Cu−MOR sample activated at increasing temperatures (from 300 to 673 K). The sample activated at room temperature (full line spectrum) exhibits the typical features of hydrated Cu^{2+} species.[8,19,30,31,36] Activation at 373 K (dashed curve) causes a red shift of about 1 eV of the 1s → $4p_{xy}$ transition (vide infra the end of this section for the discussion on the $4p_{xy}/4p_z$ splitting induced by axial symmetry). No significant copper reduction is observed at this stage, owing to the absence of the 1s → $4p_{xy}$ electronic transition of Cu^+ species in the 8983−8984 eV region. The observed shift is due to a change in the coordination sphere of Cu^{2+} species upon water desorption, as witnessed by the parallel decrease of the white line intensity and by the EXAFS analysis (vide infra section 3.1.3).

Starting from the sample activated at 473 K (dotted curve), the 1s → $4p_{xy}$ electronic transition of Cu^+ species appears at around 8983.0−8983.3 eV, and its normalized intensities progressively increase from 0.16 to 0.61 (sample activated at 673 K, bold full line; see Table 1). Note that the increase of the Cu^+ 1s → $4p_{xy}$ transition is accompanied by a parallel red shift of the edge, better appreciated from the derivative spectra reported in Figure 2b. This means that the actual reduction of

TABLE 1: Position and Related Normalized Intensities of the Main Features of the XANES Spectra of Cu−MOR Activated at Increasing Temperatures and in Different Atmosphere (from Figures 2, 5, and 8)[a]

	$1s \rightarrow 4p_x$		$1s \rightarrow 4p_y$		$1s \rightarrow 4p_z$	
	position (eV)	intensity	position (eV)	intensity	position (eV)	intensity
			Cu^+			
ZSM-5[b]	degenerate with $1s \rightarrow 4p_y$		8983.5	0.92	8986.6	0.71
MOR-473	degenerate with $1s \rightarrow 4p_y$		8983.1	0.16	8987.3	0.56
MOR-573	degenerate with $1s \rightarrow 4p_y$		8983.3	0.29	8987.1	0.56
MOR-673	degenerate with $1s \rightarrow 4p_y$		8983.0	0.61	8986.7	0.59
+NO (80 K)	8978.9 (sh)	0.07	8983.1	0.33	8986.1 (sh)	0.59
ZSM-5+NO (80 K)[c]	8979.9 (sh)	0.15	8983.7 (sh)	0.56	8986.3 (sh)	0.68

	$1s \rightarrow 4p_x$		$1s \rightarrow 4p_y$		$1s \rightarrow 4p_z$		$1s \rightarrow 3d$	
	position	intensity	position (eV)	intensity	position	intensity	position (eV)	intensity
			Cu^{2+}					
ZSM-5-300[d]	degenerate with $1s \rightarrow 4p_y$		8988.0 (sh)	0.56	in the edge		8977.8	0.04
MOR-300	degenerate with $1s \rightarrow 4p_y$		8988.8 (sh)	0.63	in the edge		8977.3	0.030
MOR-373	degenerate with $1s \rightarrow 4p_y$		8987.8 (sh)	0.58	in the edge		8977.2	0.035

[a] The first and the second part of the table refer to spectra dominated respectively by the features of Cu^+ and Cu^{2+}. The Co-presence of both oxidation states makes the values reported here somewhat qualitative. This, however, does not hold for the $1s \rightarrow 4p_y$ (often degenerate with $1s \rightarrow 4p_x$) transition of Cu^+, used to quantify the fraction of cuprous ions (see text and Table 2) because it is very strong and appears in a region where Cu^{2+} features are negligible (sh = shoulder; MOR-x = Cu−MOR activated at x K). For comparison also data referring to the Cu−ZSM-5 system were reported (from refs 22 and 36). [b] Data referring to a Cu^+−ZSM-5, prepared from gas phase exchange with CuCl, and representing a model system containing only Cu^+ ions (from ref 22). [c] Sample a after interaction with NO at 77 K (from ref 22). [d] Cu^{2+}−ZSM-5 sample prepared by ion exchange from Cu^{2+} aqueous solutions (from ref 36).

TABLE 2: Comparison of the Fraction of Cu^{2+} Sites in Cu−MOR and Cu−ZSM-5 Systems, As Probed by XANES and EPR Spectroscopies and Relative Differences (EPR-Silent Sites) as a Function of the Activation Temperature

	MOR			ZSM-5		
activation T	XANES	EPR	EPR-silent	XANES	EPR	EPR-silent
300	100	100	−	100	100	−
373	100	79	21	100	89	11
473	85	43	42	70	49	21
573	65	8	47	38	3	35
673	30	2	28	5	4	−

Cu^{2+} is taking place starting from 473 K only. To evaluate, on a semiquantitative ground, the fraction of copper ions reduced at the different stages of the activation process, the relative intensity of the $1s \rightarrow 4p_{xy}$ electronic transition of Cu^+ can be used if an appropriate reference is available. Cu^+−ZSM-5 sample, prepared by a gas-phase exchange with CuCl,[16] represents a model solid containing 100% isolated Cu^+ species in a similar local environment,[18,20−22] and can so be used as a reference. The XANES spectrum of Cu^+−ZSM-5, measured with the same instrument and in the same experimental conditions,[22] exhibits a $1s \rightarrow 4p_{xy}$ preedge peak with an intensity of 0.92, as can be observed in Figure 2a (line-square curve). From this comparison a fraction of 17, 32, and 66% of Cu^+ is inferred for the sample activated at 473, 573, and 673 K, respectively (Table 2). For the sample activated at 473 K the value of 17% of Cu^+ represents an overestimation of the actual cuprous ions percentage owing to a significant contribution of the low-energy tail of the $1s \rightarrow 4p_{xy}$ electronic transition of the dominant Cu^{2+} species; conversely, the values estimated for the sample activated at higher temperature are more accurate.

Part b of Figure 2 reports the corresponding derivatives of the XANES spectra in part a. The derivative spectrum of Cu−MOR activated at room temperature exhibits the doublet of maxima typical of Cu^{2+} species around 8987 and 8993 eV.[19,30,46,47,51] Both the maximum around 8982 eV and the minimum around 8984 eV, characteristic of Cu^+,[19,30,46,47,51] are well visible in the Cu−MOR sample when activated at 673 K and totally absent when activated at 300 and 373 K. If the intensity of the maximum of the derivative spectra is considered to evaluate the fraction of Cu^+, values of 15%, 36%, and 75% are obtained for the samples activated at 473, 573, and 673 K, respectively. These figures are slightly different (within 10%) from those evaluated from part a, which reflects the semiquantitative ground of the estimation. For the sake of brevity, only the Cu^{2+} fractions evaluated from the XANES spectra are reported in Table 2.

Even if not necessary for the redox chemistry discussed here, it is worth noticing that the high resolution of the XANES spectra reported in Figure 2a allows us to extract further information on the local symmetry of copper ions, which are of interest on a chemical physics ground. For all spectra where the fraction of Cu^+ species is appreciable, besides the already discussed preedge peak, we observe a clear shoulder in the edge, 3−4 eV blue-shifted. In agreement with ref 22 we attribute both preedge features to the splitting of the $1s \rightarrow 4p$ transition into a $1s \rightarrow 4p_{xy}$ (at 8983.0 eV for the sample activated at 673 K) and a $1s \rightarrow 4p_z$ (at 8986.7 eV for the sample activated at 673 K) components. This $4p_{xy}/4p_z$ splitting of 3.7 eV reflects the axial symmetry of Cu^+ ions and agrees with the axial symmetry observed with EPR spectroscopy for the oxidized state of copper counterions inside MOR. For Cu^+−ZSM-5 a $4p_{xy}/4p_z$ splitting of 3.1 eV was observed by high-resolution XANES experiments carried out in the same way[22] (see Table 1).

3.1.3. EXAFS. The parallel EXAFS data (Fourier transform, phase uncorrected, of the $k^3\chi(k)$ function) are reported in Figure 3a. The spectra are dominated by the Cu−O signals generating a peak in the 0.9−2.0 Å range, which contains the contributions of oxygen atoms from both the zeolite framework and adsorbed water molecules. A simple inspection of the data reported in Figure 3a indicates a reduction of the average first shell Cu−O peak upon increasing the activation temperature, reflecting the progressive elimination of H_2O molecules from the first coordination shell of copper ions. Quantitative EXAFS analysis (see Figure 3b for the quality of the fits) indicates a reduction of the Cu−O coordination number from 4.1 ± 0.4 in the sample activated at 300 K to 2.9 ± 0.3 in the sample activated at 673 K. A similar result was obtained by Kuroda and co-workers[30] for the thermal reduction of a similar Cu^{2+}−mordenite sample

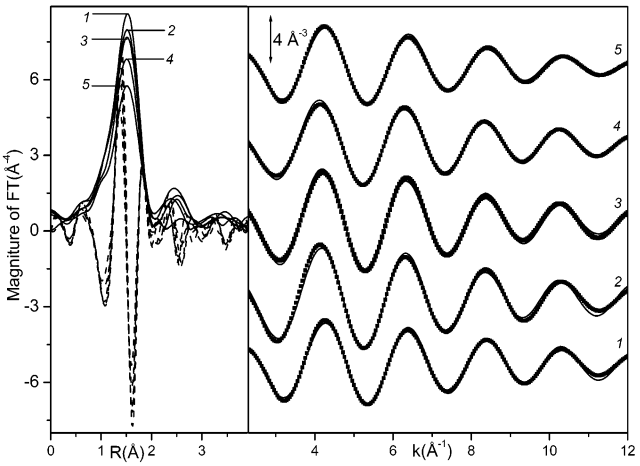

Figure 3. (a) k^3-weighted, phase-uncorrected FT of the EXAFS spectra corresponding to the sample Cu−MOR thermally treated at increasing temperatures: 300 K (1), 373 K (2), 473 K (3), 573 K (4), and 673 K (5). Modulus and imaginary parts were reported as full and dashed lines, respectively. (b) Corresponding first shell filtered data and related best fit.

(Si/Al = 10, overexchanged at 215%) where the coordination number moved from 4.2 to 3.1 for Cu^{2+}−mordenite activated at 300 and 673 K respectively, reaching the value of 2.5 for the sample activated at 873 K. In the Cu^{2+}−ZSM-5 sample reported in ref 36 the Cu−O coordination number moves from 3.9 ± 0.4 in the sample activated at 300 K to 2.3 ± 0.3 in the sample activated at 673 K. We can so conclude that copper ions exhibit a higher averaged coordination number when hosted in mordenite, at any activation temperature in the 300−673 K range. At high distances (2.0−2.9 Å range in Figure 3a) the contribution of a second Cu−O−Cu shell progressively growths up on increasing the activation temperature.

3.1.4. Summary of the EPR, XANES, and EXAFS Results and Comparison with the Cu−ZSM-5 System. As far as the Cu−MOR sample activated at 673 K is concerned, the direct comparison between the fraction of Cu^{2+} observed by EPR (2%) and by XANES (34−25%) leads to an evident contradiction. A systematic underestimation of the fraction of Cu^{2+} by EPR along the whole series of activation process is clear. This effect was already observed in the thermal reduction of the Cu^{2+}−ZSM-5 system[36] and explained in terms of formation of EPR-silent cupric species such as isolated paramagnetic Cu^{2+} in some particular low coordination state characterized by very fast relaxation or $Cu^{2+}O^{2-}Cu^{2+}$ pairs, both diamagnetic ($S = 0$) or ferromagnetic ($S = 1$), but with a very large zero field splitting because of strong distortion in the symmetry. This hypothesis will be demonstrated in the following (section 3.2.4). The existence of $Cu^{2+}O^{2-}Cu^{2+}$ pairs is evidenced by the contribution in the 2.0−2.9 Å range of the Fourier transformed EXAFS data (Figure 3a), which progressively grows up increasing the activation temperature.

The parallelism between Cu^{2+}−ZSM-5 and Cu^{2+}−MOR systems is only partial because activation at 673 K leads to a complete reduction of cupric ions in ZSM-5, as witnessed by both XANES and EPR techniques (see Table 2), whereas a significant remaining fraction (ca. 30%) is still present in mordenite, according to XANES. Moreover, the fraction of Cu^{2+} EPR-silent species (evaluated as the difference between XANES and EPR estimations) is higher in mordenite than in ZSM-5, whatever the activation temperature. This fact reflects the higher cation concentration in mordenite, facilitating the formation of $Cu^{2+}O^{2-}Cu^{2+}$ EPR-silent pairs.

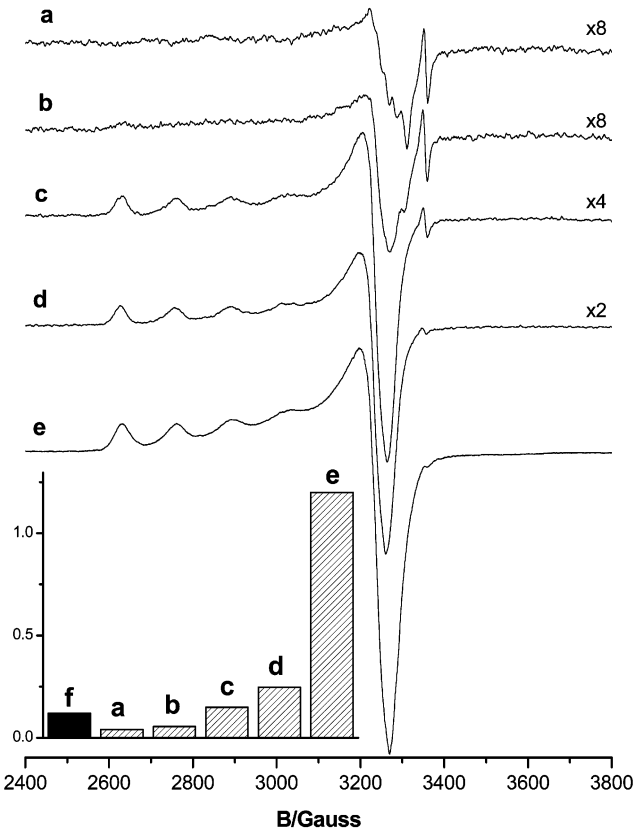

Figure 4. EPR spectra, recorded at 77 K, of Cu−MOR activated at 673 K (spectrum a) and after contact with increasing amounts of water (spectra b−d) and successive dosage of O_2 (spectrum e). The inset shows the integrated intensities of spectra a−e. A second Cu−MOR sample activated at 673 K was contacted with O_2 at room temperature and then measured at 77 K, resulting in an EPR spectrum (not reported) with an intensity corresponding to column f in the inset.

3.2. Reoxidation of Thermal Reduced Cu−MOR by H_2O and O_2. *3.2.1. EPR Spectroscopy.* After thermal reduction of the sample by outgassing at 673 K, admittance of increasing amounts of water at room temperature gradually restored the intensity of the EPR signal, up to ca. 25% of the original value for the starting Cu−MOR hydrated sample, as shown in Figure 4 (spectrum d). The resulting EPR spectrum is typical in shape and parameters of hydrated cupric species.[13,36,52,53] When the rehydrated sample was then contacted with O_2 (100 Torr) at room temperature, a complete recovery of the intensity of the EPR signal was observed (spectrum e). In this case, an intensity even higher than 1.0 is obtained. This fact is not surprising and just means that our reference sample (Cu−MOR sample activated at room temperature, spectrum a in Figure 1) contains a fraction of EPR inactive cupric species that become active upon full rehydration. It is a rather common fact that, after a redox cycle, a higher number of EPR active species, with respect to the reference sample, is found.[54,55]

Conversely, when O_2 was admitted in the fully dehydrated (reduced) sample (same conditions as above, but without previous contact with water), an increase of the EPR signal of cupric species was observed only to a minor extent; see inset of Figure 4 (point f). Therefore, rehydration of the thermally reduced sample *prior* to O_2 adsorption is necessary to observe an efficient oxidation by molecular oxygen at room temperature. In other words, oxidation of Cu^+ by molecular O_2 alone is an activated process and does not take place at room temperature.

3.2.2. XANES Spectroscopy. The most evident effect of H_2O dosage on the XANES spectrum of Cu−MOR activated at 673

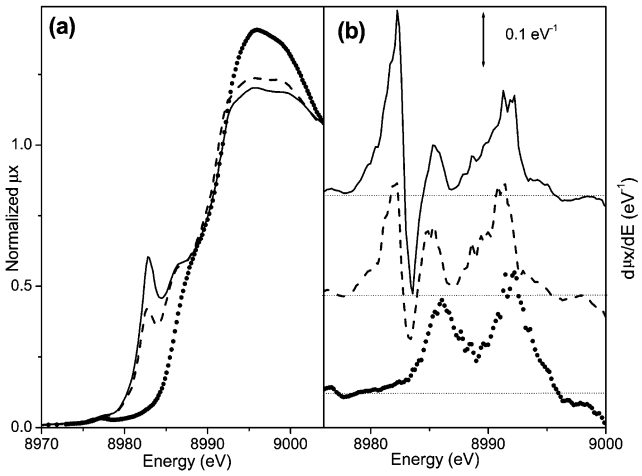

Figure 5. (a) XANES spectra of Cu−MOR thermally treated 673 K (full line), after interaction with water (dashed line, dosage comparable with that of curve d of Figure 4) and after subsequent O_2 dosage (●). (b) Corresponding derivative spectra (same drawing as in part a). For sake of clarity spectra were vertically shifted. For every curve a horizontal dotted line represents the corresponding zero level.

K (Figure 5a) is the reduction of the 1s → $4p_{xy}$ preedge peak of Cu^+ species. This effect cannot be attributed to an oxidation process owing to the absence of a parallel blue shift of the edge, but to a change of the coordination sphere due to the formation of hydrated species. This is testified by the increase of the white line and of the coordination number, 3.6 ± 0.3, obtained from the EXAFS data (spectra not reported for brevity). Note that a decrease of the 1s → $4p_{xy}$ component upon formation of adducts on cuprous species is well-known; see, for example, the case of carbonyl complexes formed inside zeolite channels.[18,21,47,56,57] Conversely, upon subsequent interaction with O_2, the XANES features of hydrated Cu^{2+} species are fully restored: disappearance of the 1s → $4p_{xy}$ preedge peak of Cu^+ species, appearance of the 1s → 3d preedge peak of Cu^{2+} species, and a 4.5 eV blue shift of the edge. The same holds in the derivative spectra reported in Figure 5b: erosion of the positive (8982 eV) and negative (8984 eV) peaks of Cu^+ species and appearance of the doublet of maxima typical of Cu^{2+} species around 8987 and 8993 eV.[19,30,46,47,51]

3.2.3. Summary of the EPR, XANES, and EXAFS Results and Comparison with the Cu−ZSM-5 System. According to both XANES and EPR, water adsorption onto the Cu−MOR sample activated at 673 K is not able to reoxidize cuprous ions to the cupric state. Therefore, the progressive increment of the EPR signal observed upon rehydration has to be attributed to the ability of H_2O molecules to disaggregate existing $Cu^{2+}O^{2-}Cu^{2+}$ pairs (amounting to ca. 30% of the whole Cu cations, see Table 2) that become EPR active. Further proof comes from the diminution of the intensity of the Cu−O−Cu component of the EXAFS signal and by the neat increment of the average coordination number of copper species evaluated from the EXAFS of the rehydrated Cu−MOR sample. A similar effect of water was already observed in the Cu−ZSM-5 system and explained in similar terms.[36] These facts are thus able to explain the apparent contradiction observed between XANES and EPR data during the thermal activation (vide supra section 3.1).

When O_2 is adsorbed at room temperature on the sample previously contacted with water, a further relevant increase of the EPR signal is observed. In this case, the increment of the EPR signal is accompanied by a definite oxidation of cuprous ions, as testified by XANES spectroscopy.

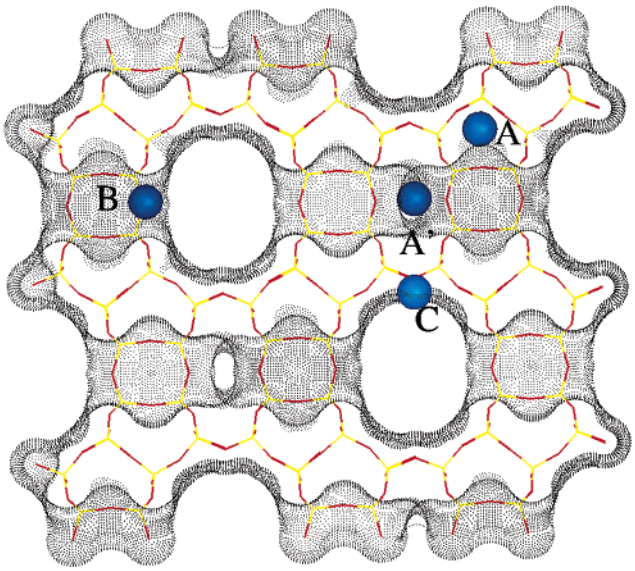

Figure 6. Computer modeling of the mordenite structure projected along the [001] direction, showing extraframework cations. Dots outline the Connolly surface[59] obtained with a probe molecule 2.8 Å in diameter.

3.3. Interaction of NO Molecules with Cu−MOR Activated at 673 K: A Temperature Dependent Study in the 77−300 K Range. For a better understanding of the oxidation state of copper species and of their environment in mordenite after thermal reduction, we conducted a combined FTIR and XAFS study of the (partially) reduced Cu−MOR sample upon interaction with NO. Before entering into the details of the spectra, a brief description of the cation distribution inside mordenite is demanded.

3.3.1. Outline of the Mordenite Structure and Cation Location. Mordenite is a zeolite with orthorhombic structure which has a set of parallel channels running along the [001] direction.[40] These channels have an elliptical cross section, 6.5 × 7.0 Å in diameter, defined by 12-membered rings of TO_4 tetrahedra. The channel wall has side pockets in the [010] direction that are accessible through windows with a free entrance of 3.9 Å in diameter. Each side pocket connects, through a distorted eight-membered ring, with two other side pockets that open into the adjacent main channel. However, there is a constriction halfway along this connection with a free diameter of about 2.6 Å. Extraframework cation sites are situated[58] on the walls of the site pockets (A), at the access to these pockets (B), on the walls of the main channels (C), and at the bottom of the side pockets (A′). This is depicted in Figure 6, which also shows the Connolly surface[59] of the zeolite (obtained with a probe molecule 2.8 Å in diameter). Note that all cations are accessible to NO molecules except for those at sites A′.

3.3.2. IR Study. Parts a and b of Figure 7 report the IR spectra, in the N−O stretching region, of increasing NO equilibrium pressures (P_{NO}) dosed at liquid nitrogen temperature on Cu−MOR sample previously activated at 673 K. For the sake of clarity, the adsorption process was divided into two parts for the low and the high P_{NO}. At the lowest P_{NO} (Figure 7a) the spectra are rather simple, showing only two bands at 1813 and 1910 cm^{-1}, which are due to the formation of mononitrosyl adducts formed on Cu^+ and Cu^{2+} sites, respectively. This reflects the co-presence of cuprous and cupric species in the thermally activated Cu−MOR sample, as already determined by the previously discussed EPR and XANES study. Upon increasing P_{NO}, the band due to $Cu^{2+}\cdots NO$ complexes increases,

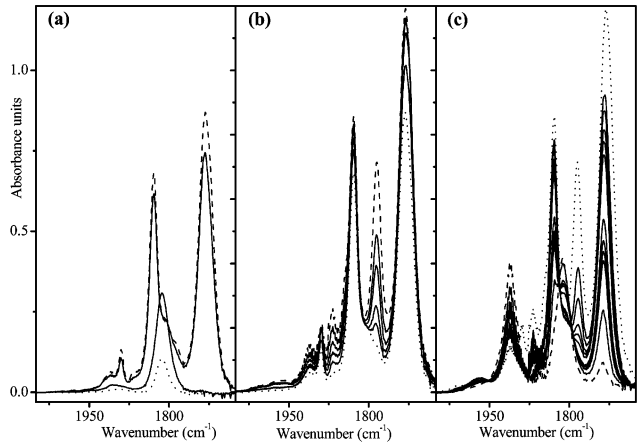

Figure 7. FTIR spectra, in the N−O stretching region, of increasing P_{NO} dosed at liquid nitrogen temperature on the Cu−MOR sample previously activated at 673 K: low and high P_{NO} are presented in (a) and (b), respectively. (c) Evolution of the IR spectra upon increasing the temperature from 77 to 300 K in the highest P_{NO} reported in (b).

whereas that due to the $Cu^+\cdots NO$ adducts reaches its maximum intensity at the second dose and then progressively disappears, together with the appearance and increase of two new components at 1828 and 1730 cm^{-1}, which are due to the symmetric and antisymmetric stretching of the $Cu^+\cdots(NO)_2$ complexes. Up to this point, the situation is completely analogous to that found upon interaction of NO with the system Cu−ZSM-5[15,16,18,22] with the only exceptions that Cu^{2+} is not observed in Cu−ZSM-5 activated in the same conditions[36] and that the fwhm of the $Cu^+\cdots NO$ adduct is larger in Cu−MOR (30 vs 22 cm^{-1}), reflecting a higher heterogeneity of the cuprous sites.

A further P_{NO} increase (Figure 7b) results in a considerable increase of the complexity of the spectra. Three main points have to be mentioned: (i) a progressive increase of the previously commented band at 1910 cm^{-1} and of the doublet at 1828 and 1730 cm^{-1} occurs, approaching saturation at the highest P_{NO}; (ii) the development of two new components at 1870 and 1785 cm^{-1} occurs in a parallel way, indicating that we are dealing with a new doublet; (iii) finally, the sharp band at 1990 cm^{-1} with a roto-vibrational structure is just due to NO molecules in the gas phase and does not add further information.

The doublet at (1828 and 1730 cm^{-1}) is attributed to $Cu^+\cdots(NO)_2$ complexes formed on sites B and C, whereas that at (1870 and 1785 cm^{-1}) corresponds to dinitrosyl formed in the site pocket, sites A (see Figure 6). The assignment of the doublet at 1828 and 1730 cm^{-1} was done in a straightforward manner on the basis of what was learned on the Cu^+−ZSM-5 system.[15,16,18,22] In fact, both the position and the relative intensity of these two $Cu^+\cdots(NO)_2$ components are very close to what observed in ZSM-5 (1826 and 1732 cm^{-1}; see left side of Scheme 1).[22] This means that the geometry of the dinitrosyl adduct must be very similar, and this can only happen in mordenite on the sites facing the main channel, i.e., sites B and C. Conversely, the doublet at 1870 and 1785 cm^{-1} must be ascribed to $Cu^+\cdots(NO)_2$ complexes with a strongly different symmetry, owing to a significant difference in the frequencies and to a very low relative intensity of the high frequency component. Apart from sites B and C, only sites A are accessible to NO, so that this doublet has to be necessarily related to dinitrosyls formed on sites A. Summarizing, at low P_{NO} (Figure 7a) NO molecules interact with Cu^+ cations hosted in A, B, and C sites of mordenite, resulting in the appearance of the band at 1813 cm^{-1}, which is slightly blue shifted and significantly

SCHEME 1

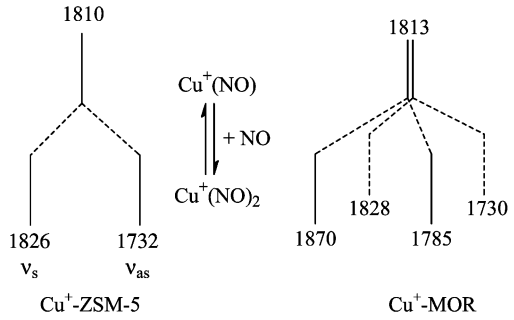

broadened with respect to that observed in the Cu^+−ZSM-5 system[18,22] (1810 cm^{-1}). This means that a single NO molecule easily interacts with and optimizes its interaction with Cu^+ cations hosted in all accessible sites, resulting in rather similar $Cu^+\cdots NO$ complexes. Upon increasing P_{NO}, $Cu^+\cdots(NO)_2$ adducts are easily formed on sites B and C, where they have the available space to optimize easily the interaction with cuprous ions, yielding to dinitrosyl complexes well comparable with those found in ZSM-5. This does not hold for cations hosted in site A (in the side pockets), where, due to steric hindrance, a second NO molecule cannot easily penetrate. Therefore, the formation of a $Cu^+\cdots(NO)_2$ complex can occur only upon a strong rearrangement of the local geometry of the cation, which has an energetic cost. This explains why in site A the $Cu^+\cdots NO \rightleftharpoons Cu^+\cdots(NO)_2$ equilibrium is displaced in favor of the mononitrosyl adduct and the dinitrosyl complex can only be observed at high P_{NO}. Scheme 1 depicts the similarities and the differences between the Cu^+−ZSM-5 and the Cu^+−MOR systems.

The evolution of the system upon increasing the temperature from 77 (dotted line) to 300 K (dashed line) is shown in Figure 7c. The decrease of the components ascribed to both $Cu^+(NO)_2$ doublets is evident, together with the parallel increase of the broad component at 1910 cm^{-1} due to due to $Cu^{2+}\cdots NO$ complexes. These changes are accompanied by the appearance of new IR features in the 2375−2200 cm^{-1} region associated with the formation of products and intermediates of the $2NO \rightarrow O_2 + N_2$ reaction. These features were already deeply discussed for the Cu−ZSM-5 system[15,16,18,22] and are not shown here for the sake of brevity. These are the IR proofs that, during the temperature increase, the NO decomposition reaction is progressively switched on, and cuprous ions are oxidized to the cupric state. The reoxidation of cuprous ions by NO is only partial, as testified by the presence of (i) the intense band at 1813 cm^{-1} due to $Cu^+\cdots NO$ complexes in sites A, B and C and (ii) the weak band at 1730 cm^{-1} and the shoulder at 1828 cm^{-1} due to $Cu^+\cdots(NO)_2$ complex in sites B and C.

3.3.3. XANES, EXAFS, and EPR Study. The inset in Figure 8a reports the EPR spectrum of the $Cu^+\cdots NO$ adducts formed on A, B, and C sites of MOR upon interaction with NO at 77 K. The adopted P_{NO} was 0.1 Torr, properly selected as a compromise to minimize both $Cu^+\cdots(NO)_2$ EPR inactive complexes and unengaged Cu^{2+} sites, which would interfere with the $Cu^+\cdots NO$ signal. Notwithstanding this caution, traces of residual Cu^{2+} ions (less than 10%) are still visible, but the dominant signal is that corresponding to the mononitrosyl adducts. Though less resolved, the spectrum in Figure 8a has the structure of that observed in the case of Cu−ZSM-5.[13,38] The main signal is typical of a low-symmetry NO adduct on Cu^+ with bent structure and with the unpaired electron mainly localized on the NO moiety. The relevant Cu hyperfine structure ($A_1 = 160 \pm 2$, $A_2 = 155 \pm 2$, $A_3 = 200 \pm 2$ G) mainly derives

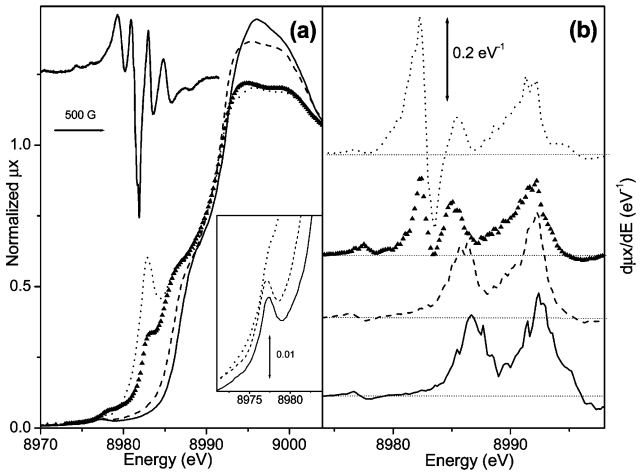

Figure 8. (a) XANES spectra of Cu−MOR thermally treated at 673 K (dotted line) and after interaction with NO at 77 K (▲, $P_{NO} = 8$ Torr). The system was then allowed to reach in NO atmosphere at room temperature and was subsequently outgassed (dashed line). For comparison also the spectrum of the starting Cu−MOR sample outgassed at room temperature is included (full line). (b) reports the corresponding derivative spectra (same drawing as in part a). For the sake of clarity, the spectra were vertically shifted. For every curve a horizontal dotted line represents the corresponding zero level. The inset in (a) corresponds to the EPR spectrum of the Cu−MOR sample thermally treated at 673 K in interaction with NO ($P_{NO} = 0.1$ Torr) at 77 K.

from spin polarization of Cu 4s orbital. The **g** and **A** tensors are typical of monoclinic symmetry ($g_{xx} \neq g_{yy} \neq g_{zz}$; $A_{xx} \neq A_{yy} \neq A_{zz}$) and the *N* hyperfine (which is smaller than that of Cu) is not resolved. The EPR study thus revealed that copper species undergo a reduction of the local symmetry from axial to monoclinic upon formation of mononitrosyl adduct.

The main body of Figure 8a reports the effect of the interaction at liquid nitrogen temperature of NO with Cu−MOR activated at 673 K on the XANES spectrum (compare dotted and ▲ spectra). To simplify the complexity of the signal, a high P_{NO} (8 Torr) was adopted, to maximize the fraction of $Cu^{+}\cdot\cdot\cdot(NO)_2$ complexes, and to minimize the complementary fraction of $Cu^{+}\cdots NO$ complexes and unengaged copper ions. As was the case for Cu^{+}−ZSM-5,[22] this interaction results in the formation of cuprous dinitrosyl adducts without measurable oxidation effects. As already observed by EPR, coordination with NO causes the loss of the axial symmetry, here observed by the splitting of the $1s \rightarrow 4p_{xy}$ into the two $1s \rightarrow 4p_x$ and $1s \rightarrow 4p_y$ components at 8978.9 and 8983.1 eV, the $1s \rightarrow 4p_z$ component being nearly unaffected (∼8986.1 eV). This results in a p_x/p_y and p_y/p_z splitting of 3.2 and 3.0 eV, respectively. In Cu^{+}−ZSM-5 the formation of $Cu^{+}\cdots(NO)_2$ complexes at liquid nitrogen temperature resulted in a p_x/p_y and p_y/p_z splitting of 3.8 and 2.6 eV, respectively.[22]

To allow the catalyst to work, the temperature was raised to 300 K; then the system was outgassed and a further XANES spectrum was collected (dashed line in Figure 8). By comparing this spectrum with our reference for a 100% Cu^{2+}−MOR (virgin sample activated at 300 K, solid curve), we can conclude that NO is able to reoxidize most of the cuprous ions in MOR, in agreement with the IR study. This fact is testified by the blue shift of the edge, by the disappearance of the $1s \rightarrow 4p_{xy}$ features of Cu^{+} species and by the recovery of the $1s \rightarrow 3d$ component of Cu^{2+} (see inset in Figure 8a). The same effects can be appreciated in the derivative spectra reported in Figure 8b.

4. Conclusions

The coordination and redox chemistry of copper species hosted in MOR zeolite under different conditions were investigated by EPR, XANES, EXAFS, and IR spectroscopies. Thermal activation below 473 K causes only the desorption of water molecules from cupric ions, accompanied by a partial aggregation in $Cu^{2+}-O-Cu^{2+}$ complexes. Starting from the sample activated at 473 K the $Cu^{2+} \rightarrow Cu^{+}$ reduction mechanism starts to be progressively operative. Conversely to that observed for Cu−ZSM-5, the reduction process is not complete for the sample activated at 673 K, where a fraction of 30% of cupric ions is still present. The presence of (EPR inactive) $Cu^{2+}-O-Cu^{2+}$ complexes, witnessed by EXAFS, explains the systematic underestimation of the fraction of Cu^{2+} species evaluated by EPR, with respect to that obtained from XANES. Interaction with water at room temperature does not cause oxidation of the system and the increase, in such conditions, of the EPR spectral intensity is related to dispersion and coordination of previously silent Cu^{2+} species. A second role of water, however, is to facilitate the reoxidation of the system by molecular oxygen assisting reoxidation. This fact explains the poisoning effect of water in the deNO_x activity of Cu-exchanged zeolites. The coordination of NO molecules on the Cu^{+}−MOR system, activated at 673 K, was studied in situ at liquid nitrogen temperature, resulting in the formation of mononitrosyl adducts on both cupric and cuprous ions, the latter evolving upon increasing P_{NO} into two distinct $Cu^{+}(NO)_2$ complexes. The XANES spectrum of such dinitrosyl adducts presents three resolved components ascribed to the $1s \rightarrow 4p_x$, $1s \rightarrow 4p_y$, and $1s \rightarrow 4p_z$ transitions, the p_x/p_y and p_y/p_z splittings being 3.2 and 3.0 eV, respectively. This testifies to the rupture of the axial symmetry of Cu^{+} bare cations upon NO adsorption. The deNO_x chemistry was then switched on by allowing the system to reach room temperature in a NO atmosphere. In all stages of this study, comparison is made with a Cu^{+}−ZSM-5 model system.[22,36] The differences observed between these two systems are explained in terms of the different structural (cation concentration and environment) characteristics.

Acknowledgment. We are indebted to T. Yamamoto and C. Otero Areán for fruitful discussion, and with the staff of the GILDA BM8 beamline at the ESRF (in particular with F. D'Acapito) for the important support during XANES measurements (experiment CH-1015 November 28-December 03, 2001). The cell used for performing in situ XANES measurements at 80 K under controlled atmosphere was designed in collaboration with the staffs of the GILDA beamline and INFM OGG in Grenoble (F. Danca, F. La Manna, and R. Felici) and supported by INFM PURS project.[44] The Secretaría de Estado de Educación y Universidades of Spain is acknowledged for a postdoctoral grant to F.X.L.X.

References and Notes

(1) Iwamoto, M.; Furukawa, H.; Mine, Y.; Uemura, F.; Mikuyira, S.; Kagawa, S. *J. Chem. Soc., Chem. Commun.* **1986**, 1272.

(2) Iwamoto, M.; Yahiro, H.; Mine, Y.; Kagawa, S. *Chem. Lett.* **1989**, 213.

(3) Iwamoto, M.; Yahiro, H.; Kutsuno, T.; Bunyo, S.; Kagawa, S. *Bull. Chem. Soc. Jpn.* **1989**, *62*, 583.

(4) Iwamoto, M.; Yahiro, H.; Tanda, K.; Mizuno, N.; Mine, Y.; Kagawa, S. *J. Phys. Chem.* **1991**, *95*, 3727.

(5) Iwamoto, M.; Yahiro, H.; Mizuno, K. N.; Zhang, Y. W. X.; Mine, Y.; Kagawa, S. *J. Phys. Chem.* **1992**, *96*, 9360.

(6) Yamashita, H.; Matsuoka, M.; Tsuji, K.; Shioya, Y.; Anpo, M.; Che, M. *J. Phys. Chem.* **1996**, *100*, 397.

(7) Hamada, H.; Matsubayashi, N.; Shimada, H.; Kintaichi, Y.; Ito, T.; Nishijima, A. *Catal. Lett.* **1990**, *5*, 189.

(8) Grünert, W.; Hayes, N. W.; Joyner, R. W.; Shpiro, E. S.; Rafiq, M.; Siddiqui, H.; Baeva, G. N. *J. Phys. Chem.* **1994**, *98*, 10832.
(9) Kharas, K. C. C. *Appl. Catal. B* **1993**, *2*, 207.
(10) Liu, D.-J.; Robota, H. J. *Appl. Catal. B* **1994**, *4*.
(11) Kharas, K. C. C.; Liu, D.-J.; Robota, H. J. *Catal. Today* **1995**, *26*, 129.
(12) Kumashiro, R.; Kuroda, Y.; Nagao, M. *J. Chem. Phys. B* **1999**, *103*, 89.
(13) Giamello, E.; Murphy, D.; Magnacca, G.; Morterra, C.; Shioya, Y.; Nomura, T.; Anpo, M. *J. Catal*. **1992**, *136*, 510.
(14) Beutel, T.; Sàrkàny, J.; Lei, G.-D.; Yan J. Y.; Sachtler, W. M. H. *J. Phys. Chem.* **1996**, *100*, 845.
(15) Spoto, G.; Bordiga, S.; Scarano D.; Zecchina, A. *Catal. Lett.* **1992**, *13*, 39.
(16) Spoto, G.; Zecchina, A.; Bordiga, S.; Ricchiardi, G.; Martra, G.; Leofanti G.; Petrini, G. *Appl. Catal. B* **1994**, *3*, 151.
(17) Spoto, G.; Bordiga, S.; Ricchiardi, G.; Scarano, D.; Zecchina, A.; Geobaldo, F. *J. Chem. Soc., Faraday Trans.* **1995**, *91*, 3285.
(18) Lamberti, C.; Bordiga, S.; Salvalaggio, M.; Spoto, G.; Zecchina, A.; Geobaldo, F.; Vlaic, G.; Bellatreccia, M. *J. Phys. Chem. B* **1997**, *101*, 344.
(19) Lamberti, C.; Spoto, G.; Scarano, D.; Pazé, C.; Salvalaggio, M.; Bordiga, S.; Zecchina, A.; Turnes Palomino G.; D'Acapito, F. *Chem. Phys. Lett*. **1997**, *269*, 500.
(20) Zecchina, A.; Bordiga, S.; Turnes Palomino, G.; Scarano, D.; Lamberti, C.; Salvalaggio, M. *J. Phys. Chem. B* **1999**, *103*, 3833.
(21) Lamberti, C.; Turnes Palomino, G.; Bordiga, S.; Berlier, G.; D'Acapito, F.; Zecchina, A. *Angew. Chem., Int. Ed.* **2000**, *39*, 2138.
(22) Prestipino, C.; Berlier, G.; Llabrés i Xamena, F. X.; Spoto, G.; Bordiga, S.; Zecchina, A.; Turnes Palomino, G.; Yamamoto, T.; Lamberti, C. *Chem. Phys. Lett.* **2002**, *363*, 389.
(23) Rodriguez-Santiago, L.; Sierka, M.; Branchadell, V.; Sodupe, M.; Sauer, J. *J. Am. Chem. Soc.* **1998**, *120*, 1545.
(24) (a) Nachtigallova, D.; Nachtigall, P.; Sierka, M.; Sauer, J. *Phys. Chem. Chem. Phys*. **1999**, *1*, 2019. (b) Nachtigallova, D.; Nachtigall, P.; Sauer, J. *Phys. Chem. Chem. Phys*. **2001**, *3*, 1552.
(25) (a) Nachtigall, P.; Nachtigallova, D.; Sauer, J. *J. Phys. Chem. B* **2000**, *104*, 1738. (b) Nachtigall, P.; Davidova, M.; Nachtigallova, D. *J. Phys. Chem. B* **2001**, *105*, 3510.
(26) Li, Y.; Keith Hall, W. *J. Catal.* **1991**, *129*, 202.
(27) Sàrkàny, J.; d'Itri, J. L.; Sachtler, W. M. H. *Catal. Lett.* **1992**, *16*, 241.
(28) Keith Hall, W.; Vaylon, J. *Catal. Lett.* **1992**, *15*, 311.
(29) Vaylon, J.; Keith Hall, W. *J. Phys. Chem.* **1993**, *97*, 7054.
(30) Kuroda, Y.; Yoshikawa, Y.; Konno, S.; Hamano, H.; Maeda, H.; Kumashiro, R.; Nagao, M. *J. Phys. Chem.* **1995**, *99*, 10621.
(31) Kuroda, Y.; Maeda, H.; Yoshikawa, Y.; Kumashiro, R.; Nagao, M. *J. Phys. Chem. B* **1997**, *101*, 1321.
(32) Jong, H. J.; Keith Hall, W.; d'Itri, J. L. *J. Phys. Chem.* **1996**, *100*, 9416.
(33) Cheung, T.; Bhargava, S. K.; Mobday, M.; Forger, K. *J. Catal.* **1996**, *158*, 301.
(34) Larsen, S. C.; Aylor, A.; Bell, A.; Reimer, J. A. *J. Phys. Chem.* **1994**, *98*, 11533.
(35) Lo Jacono, M.; Fierro, G.; Dragone, R.; Feng, X.; d'Itri, J.; Keith Hall, W. *J. Phys. Chem.* **1997**, *101*, 1979.
(36) Turnes Palomino, G.; Fisicaro, P.; Bordiga, S.; Zecchina, A.; Giamello, E.; Lamberti, C. *J. Phys. Chem. B* **2000**, *104*, 4064.
(37) Lei, G. D.; Adelman, B. J.; Sàrkàny, J.; Sachtler, W. M. H. *Appl. Catal. B* **1995**, *5*, 245.
(38) Sojka, Z.; Che, M.; Giamello, E. *J. Phys. Chem. B* **1997**, *101*, 4831.
(39) Lamberti, C.; Bordiga, S.; Zecchina, A.; Salvalaggio, M.; Geobaldo, F.; Otero Areán, C. *J. Chem. Soc., Faraday Trans*. **1998**, *94*, 1519.
(40) (a) Meier, W. M.; Olson, D. H. *Atlas of Zeolite Structure Types*, Butterworth: London, 1987. (b) Szostak, R. M. *Molecular Sieves*; Van Nostrand Reinhold: New York, 1989.
(41) (a) Zecchina, A.; Otero Areán, C. *Chem. Soc. Rev*. **1996**, *25*, 187. (b) Knözinger, H.; Huber, S. *J. Chem. Soc., Faraday Trans*. **1998**, *94*, 2047. (c) Zecchina, A.; Spoto, G.; Bordiga, S. in *Handbook of vibrational spectroscopy*; Chalmers, J. M.; Griffiths, P. R. Eds.; John Wiley & Sons Ltd.: Chichester, UK, 2002; pp 3042−3071.
(42) Lamberti, C.; Bordiga, S.; Zecchina, A.; Palin, L.; Capello, L.; Turnes Palomino, G.; D'Acapito, F. *ESRF Proposal CH-1015*, BM8 GILDA beamline, November 28, December 3, 2001.
(43) Pascarelli, S.; Boscherini, F.; D'Acapito, F.; Meneghini, C.; Hrdy J.; Mobilio, S. *J. Synchrotron Rad.* **1996**, *3*, 147.
(44) Lamberti, C.; Prestipino, C.; Bordiga, S.; Berlier, G.; Spoto, G.; Zecchina, A.; Laloni, A.; La Manna, F.; Danca, F.; Felici, R.; D'Acapito, F.; Roy, P. *Nucl. Instrum. Methods B* **2003**, *200*, 196.
(45) Lytle, F. W.; Sayers, D. E.; Stern, E. A. *Physica B* **1989**, *158*, 701.
(46) Kuroda, Y.; Kotani, A.; Maeda, H.; Moriwaki, H.; Morimato, T.; Nagao, M. *J. Chem. Soc., Faraday Trans.* **1992**, *88*, 1583.
(47) Kumashiro, R.; Kuroda, Y.; Nagao, M. *J. Phys. Chem. B* **1999**, *103*, 89.
(48) Liu, D.-J.; Robota, H. J. *Catal. Lett.* **1993**, *21*, 291.
(49) Bolis, V.; Maggioroini, S.; Meda, L.; D'Acapito, F.; Turnes Palomino, G.; Bordiga, S.; Lamberti, C. *J. Chem. Phys*. **2000**, *113*, 9248.
(50) (a) Kau, L. S.; Spira-Solomon, D. J.; Penner-Hahn, J. E.; Hodgson, K. O.; Solomon, E. I. *J. Am. Chem. Soc.* **1987**, *109*, 6433. (b) Blackburn, N. J.; Strange, R. W.; Reedijk, J.; Volbeda, A.; Farooq, A.; Karlin, A.; Zubieta, J. *Inorg. Chem.* **1989**, *28*, 1349.
(51) (a) Lamberti, C.; Prestipino, C.; Bonino, F.; Capello, L.; Bordiga, S.; Spoto, G.; Zecchina, A.; Díaz Moreno, S.; Cremaschi, B.; Garilli, M.; Marsella, A.; Carmello, D.; Vidotto, S.; Leofanti, G. *Angew. Chem., Int. Ed.* **2002**, *41*, 2341. (b) Prestipino, C.; Bordiga, S.; Lamberti, C.; Vidotto, S.; Garilli, M.; Cremaschi, B.; Marsella, A.; Leofanti, G.; Fisicaro, P.; Spoto, G.; Zecchina, A. *J. Phys. Chem. B* **2003**, *107*, 5022.
(52) Nicula, A.; Stamires, D.; Turkevich, J. *J. Phys. Chem*. **1965**, *42*, 3684.
(53) Chao, C. C.; Lunsord, J. H. *J. Phys. Chem.* **1972**, *74*, 178.
(54) Leofanti, G.; Marsella, A.; Cremaschi, B.; Grilli, M.; Zecchina, A.; Spoto, G.; Bordiga, S.; Fisicaro, P.; Prestipino, C.; Villain, F.; Lamberti, C. *J. Catal.* **2002**, *205*, 375.
(55) Berlier, G.; Spoto, G.; Fisicaro, P.; Bordiga, S.; Zecchina, A.; Giamello, E.; Lamberti, C. *Microchem. J.* **2002**, *71*, 101.
(56) Turnes Palomino, G.; Bordiga, S.; Zecchina, A.; Marra, G. L.; Lamberti, C. *J. Phys. Chem. B* **2000**, *104*, 8641.
(57) Turnes Palomino, G.; Zecchina, A.; Giamello, E.; Fisicaro, P.; Berlier, G.; Lamberti, C.; Bordiga, S. *Stud. Surf. Sci. Catal*. **2000**, *130*, 2915.
(58) (a) Attfield, M. P.; Weigel, S. J.; Cheetham, A. K. *J. Catal*. **1997**, *170*, 227. (b) Mortier, W. J. *Compilation of Extraframework Sites in Zeolites*; Butterworth: London, 1981.
(59) (a) Connolly, M. L. *Science* **1983**, *221*, 707. (b) Bordiga, S.; Ricchiardi, G.; Spoto, G.; Scarano, D.; Carnelli, L.; Zecchina, A.; Otero Areán, C. *J. Chem. Soc., Faraday Trans.* **1993**, *89*, 1843.